Exchange-bias-like coupling in a ferrimagnetic Fe/Tb multilayer

Amitesh Paul,* Saumya Mukherjee, Wolfgang Kreuzpaintner, and Peter Böni
Technische Universität München, Physik-Department E21, Lehrstuhl für Neutronenstreuung, James-Franck-Strasse 1, D-85748 Garching b. München, Germany

(Received 14 November 2013; revised manuscript received 1 April 2014; published 16 April 2014)

Field cooling of a transition metal-rare earth (TM-RE) Fe/Tb-multilayer system is shown to form a double hysteresis loop with exchange-bias-like shifts along and opposite to the field cooling axis below the ordering temperature of the RE. The measurement of the polarized neutron reflectivity at various applied fields confirms an antiferromagnetic alignment between the individual layers of Fe and Tb associated with a significant value of the magnetic moment for the Tb layers, even at room temperature. We attribute the shifts of the hysteresis loops to the formation of 2π-domain walls by the interface moments that are pinned by the magnetically hard Tb layers forming bidomainlike states in this layered artificial ferrimagnetic system. We conclude that the exchange bias in Fe/Tb-multilayers, the RE layers being on either sides of the TM layers, is caused by the formation of 2π-domain walls in the Fe layers thus excluding an explanation in terms of π-domain walls, which are believed to be responsible for the exchange bias in other RE-TM bilayer systems.

DOI: 10.1103/PhysRevB.89.144415 PACS number(s): 75.30.Gw, 75.70.−i

I. INTRODUCTION

The discovery of perpendicular magnetic anisotropy (PMA) in rare-earth (RE)/transition metal (TM) multilayers instigated an extensive study due to their high technological potential as magneto-optic recording media [1]. The extensive research on the origin of the PMA was enriched by the observation of interface induced PMA in Tb/Fe multilayers. As a consequence of the different atomic radii and surface energies of Tb and Fe, respectively, it was shown that different structures of top (smooth and crystalline bcc Fe) and bottom interfaces (rough and amorphous) of a multilayer influence the magnetic properties differently [2]. PMA has also been seen as a combined effect of the stress in the bulk of layers and the interfacial roughness [3]. One should note the typical thickness for which Fe/Tb multilayers show PMA is around 0.5–3.0 nm for Fe and 1.5–2.0 nm for Tb. The out-of-plane shape anisotropy is reduced for thicker films and therefore a smaller out-of-plane field or anisotropy is required to pull the magnetization out of the film plane.

When a ferromagnet/antiferromagnet (FM/AF) bilayer is cooled in an external magnetic field below the blocking temperature of the AF (T_B), a direct exchange coupling between the FM and AF layers gives rise to a shift of the magnetization loop of the FM layer along the field axis but opposite to the cooling field direction. This shift of the loop center away from zero external field is termed negative *exchange bias* field H_{eb} and commonly found in Co-CoO, IrMn-CoFe, and many other such combinations [4,5]. Apart from the usual negative exchange bias shifts, positive exchange bias (shift of the loop in the direction of the cooling field) has been observed in systems with biaxial anisotropies such as Fe/FeF_2 [6] and Co/Pt systems [7].

FM-AF bilayer systems can also be manufactured from transition metals and rare-earth metals. RE elements such as Gd, Sm, Dy, and Tb have already been used to form ferrimagnetic alloys with FM elements, which become coupled to alloys to obtain exchange bias effects [8,9]. In ferro-/ferrimagnetic rare-alloy systems such as CoNi/Gd [10], $Co/CoGd_2$ [11], and TbFe/NiFeMo [12], both positive and negative exchange bias has been reported earlier as the systems cross over from a negative shift above the compensation point to a positive shift below the compensation point of the ferrimagnetic alloy. It was proposed that (for example, in the CoNi/Gd system) the layer with a larger magnetization determines the bias direction. The coupling can vary from ferromagnetic (negative bias) to antiferromagnetic (positive bias) depending upon the interface dilution, which can effectively weaken the RE magnetization.

In a more complicated alloyed $Gd_{40}Fe_{60}/Tb_{12}Fe_{88}$ exchange-coupled bilayer system, both negative and positive H_{eb} ($\approx\pm 0.1$ kOe) depending on the cooling field have been observed [13]. In this case, the bilayers exhibit soft ferrimagnetic/hard ferrimagnetic bilayer configurations where TbFe acts as the pinning layer. It has been shown that reversal of the soft layer induces a magnetic domain wall (DW) at the interface. In conventional AF-FM systems, the interface DW develops in the AF, whereas in the FM-RE system the DW resides in the soft FM owing to the strong anisotropy in the RE. In the $Gd_{40}Fe_{60}/Sn_{45}Fe_{55}$ ferri/ferromagnetic system, both layers are soft and the total magnetization of the system remains AF coupled in zero field. It has been shown that the minor hysteresis loop reversal coincides with the creation or annihilation of a 180°-DW at the interface and within the magnetically softer FeSn layer due to the lower DW energy [8].

REs are often characterized by various magnetic phases at different temperatures. Bulk Tb, for example, changes from the paramagnetic (PM) to the AF phase at around 227 K and exhibits a helical-AF structure between 229 and 221 K. Below 213 K, Tb is FM. Thus it is expected that RE-TM systems will show exchange coupling at temperatures, where the RE exists in the AF phase. The main advantage of using a RE is that the evolving net magnetization or magnetic phases with temperature which may not be practically zero in the FM phase (unlike that in a normal AF with uncompensated moments) and thus can be monitored more efficiently. This is because they can be followed independently with temperature by a depth

*Corresponding author: amitesh.paul@frm2.tum.de

 ©2014 American Physical Society

sensitive vector-magnetometric technique such as polarized neutron scattering. However, the complicated spin structure in RE systems may make the system behave in a complex manner. Moreover, REs usually order antiferromagnetically only in a small range of temperatures which is restricted to a few tens of Kelvin below room temperature. The range varies obviously from one RE to the other and also when the REs are in thin-film form. The range may also depend on the thickness of the layer which in turn may be related to the periodicity of their inherent helical ordering. It may be interesting to note that even though the magnitude of H_{eb} in RE-transition metal systems is particularly large its explanation may contain rich fundamental aspects and has remained almost unexplored probably because of its lack of potential applications.

In this paper, we report on field cooling experiments of Fe/Tb multilayers showing in-plane magnetic anisotropy. We observe antiferromagnetic coupling between the Tb and Fe layers below 150 K. Thus the Fe/Tb system effectively represents a layered artificial ferrimagnet. It shows double hysteresis loops (DHLs) with anomalously large H_{eb}-like shifts along the negative and positive field cooling axes. We use polarized neutron reflectivity which is an effective tool to probe such challenging ferrimagnetic systems. The Tb layers at room temperature (300 K) have induced magnetic moments. The temperature evolution of the coercivities and the PNR data along with model simulations do not indicate of a decoupled system showing the DHLs. The loop shifts are attributed to the formation of bidomain-like states in the AF layers that are larger than the FM domains. Further, we can rule out the possibility of formation of a commonly observed 180°-domain walls in the softer Fe layers, pinned by the harder Tb layers. We argue that the formation of 2π-DWs within the Fe layers are responsible for the exchange bias.

II. SAMPLES AND CHARACTERIZATIONS

We have prepared two samples by dc magnetron sputtering using Si(100) as substrate, namely, (i) a thin film of Tb (d_{Tb} = 50 nm) and (ii) a multilayer consisting of five bilayers Fe/Tb, i.e., [Fe(3.0 nm)/Tb(6.0 nm)]$_5$/Fe(4.5 nm). The thickness of the layers is chosen such that the anisotropy is confined to the film plane. During deposition, the Ar pressure in the magnetron sputtering chamber was 3×10^{-3} mbar. The process was started at a chamber base pressure of 1×10^{-7} mbar.

Conventional in-plane magnetization loops are measured at various temperatures and fields using a superconducting quantum interference device (SQUID) from Quantum Design. X-ray reflectivity (XRR) measurements on a Siemens D5000 powder diffractometer provide information on the thickness and interface roughness of the layers. X-ray diffraction (XRD) patterns and atomic form microscopy (AFM) confirm the polycrystalline and granular nature of the films (not shown).

Polarized neutron reflectometry (PNR) measurements were performed at the instrument TREFF at Forschungs-Neutronenquelle Heinz Maier-Leibnitz (FRM II), Technische Universität München. The neutron wavelength was $\lambda = 4.8$ Å. An in-plane magnetic field of 5.0 kOe was applied to saturate the FM layer. The samples were first measured at 300 K in presence of various applied fields along the branch opposite to the saturating field. The samples were then cooled in presence of that saturating field (now being the cooling field) down to 50 K from 300 K before they were measured again at various fields. The magnetic field, perpendicular to the scattering plane was produced with an electromagnet. The scattered neutrons were detected by a position sensitive detector (PSD). The data treatment was conducted using in-house software.

III. RESULTS AND DISCUSSION

A. Magnetization measurements: Bulk and thin film Tb

1. Magnetization versus temperature

The temperature dependence of the magnetization as measured at various fields after zero-field cooling (ZFC) and field cooling (FC) up to 50 kOe is shown in Fig. 1 for the 50 nm Tb thin film (a) and for bulk Tb (b). For the latter we used 0.26 mg powder scrapped from the Tb target used for the film deposition. The SQUID data show a ferromagnetic behavior.

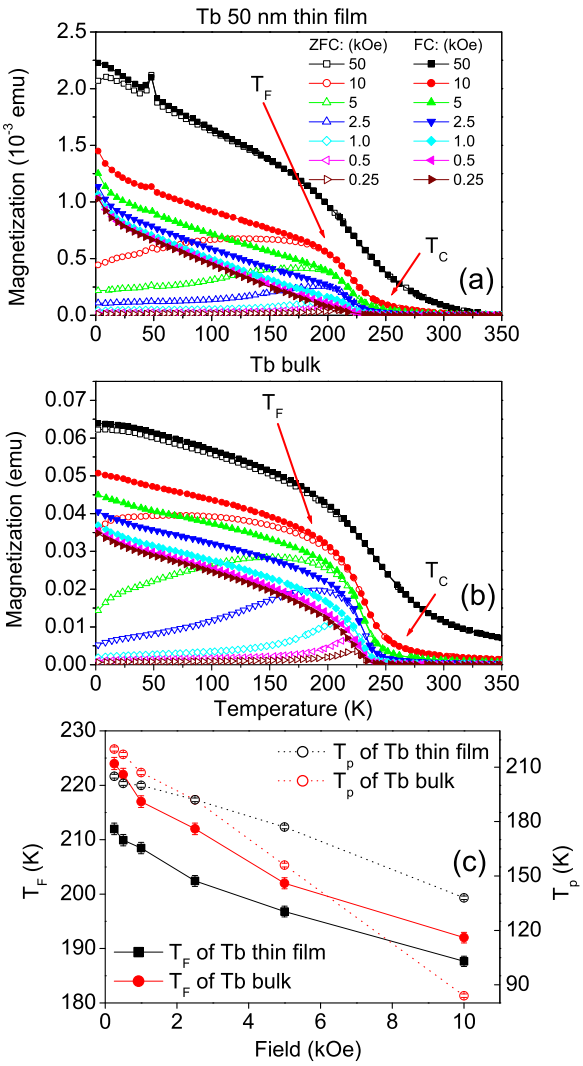

FIG. 1. (Color online) Magnetization vs temperature measurements are shown for FC and ZFC for (a) a Tb film with a thickness of 50 nm and (b) bulk Tb measured for different in-plane fields. (c) Plot of T_F and T_p vs field as obtained from the magnetization measurements shown in (a) and (b).

Similar behavior of Tb layers has been reported earlier by Svalov *et al.* [14] where they saw similar ferromagnetic behavior for films thicker than 6.0 nm.

Magnetization behavior in Tb, in general, has often been interpreted in terms of spin glasses [15] or due to strong crystalline magnetic anisotropy of Tb at low temperature [16]. Note that the FC magnetizations in Tb are often regarded as "high-field spontaneous magnetization," instead of a saturation magnetization in a normal ferromagnet due to the high anisotropy of grains in the sample [17]. It is well known that the initial permeability of a ferromagnet increases with increasing temperature and appears as a sharp peak (with a typical FWHM of 50 K) known as the Hopkinson peak just below the ordering temperature. The accepted explanation of the Hopkinson effect is based only on domain-wall motion [18]. However, in our system, we do not see such spin-glass type of behavior (confirmed from the frequency dependent ac susceptibility measurements of the bulk sample) nor such sharp Hopkinson peak. Instead, the broad peaks in the ZFC curves—commonly known as the temperature of irreversibility, are typical from a distribution of grains/domains with different anisotropic orientations of the polycrystalline grains (confirmed from the XRD measurements) of few nanometers.

The broad maxima in the ZFC curves (T_p) and furcation points of FC and ZFC curves (T_F) hve been plotted with measuring field in Fig. 1(c) for the $d_{Tb} = 50$ nm thin film and bulk sample. They both have a similar field dependence. The T_F's decrease while the onset of magnetization (around 250 K) increases with increasing in-plane field. This confirms that the thermal fluctuations are overcome more easily at lower temperatures and in large fields. The applied magnetic field favors an ordered regime, moving the onset of the freezing process to lower temperatures [19]. At 50 kOe, the antiferromagnetic ordering in Tb is presumably broken. Therefore the ZFC and FC curves gradually merge. T_F is reduced in magnitude in the Tb film as compared to bulk. Comparing these results we find that the T_F bulk (190–225 K) is close to the T_F film (185–215 K). These are, surprisingly, of the order of the helical-AF ordering temperature or the magnetic ordering temperature ($T_N = 227$ K), from the paramagnetic phase to the sinusoidal (helical) antiferromagnetic phase of Tb (usually observed in bulk). A small kink can be seen around 50 K, which happens to be a well-known artifact observed for SQUID measurements due to trapped oxygen in the sample holder.

B. Magnetization measurements: Fe/Tb multilayer

1. Magnetization versus temperature

The transition from ferromagnetism to superparamagnetism is generally expected for discrete small clusters where the individual magnetic moments within such clusters are thermally unstable. If the particle size is sufficiently small, thermal fluctuations dominate above the average blocking temperature of the nanoclusters and particles can spontaneously switch their magnetization from one easy axis to another. These directions are separated by ΔE or the anisotropy barrier. It is given by $K_A V$, where V is the average cluster volume and K_A is the anisotropy energy. When an ensemble of clusters is cooled in a zero field, lower than average blocking temperature,

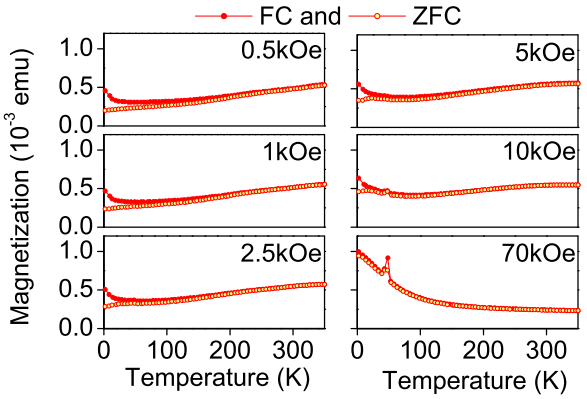

FIG. 2. (Color online) Magnetization of $[Fe/Tb]_5$ vs temperature for FC and ZFC. The external field was applied in the plane of the film.

the net moment tends to zero. When a small field is applied, the clusters with a lower blocking temperature (lower than the average blocking temperature) reach their thermal equilibrium and the sample gains a small net moment. With increasing temperature more and more clusters become unblocked and this leads to an increase in the net moment. With further increase in temperature, the net moment of the unblocked clusters (superparamagnetic) decreases following Curies's $\frac{1}{T}$ law. This gives rise to a peak in zero-field cooled magnetization with temperature. With increasing fields of measurements there is a shift of the blocking temperature due to a decrease in the energy barrier.

Figure 2 shows the temperature dependence of the magnetization as measured for ZFC and FC for fields in the range 0.5 kOe $\leqslant H \leqslant$ 70 kOe. The magnetic behavior of Fe/Tb multilayer is seen quite different from that of a single Tb thin film or Tb in bulk form. No T_p's are evident in the ZFC curves of the Fe/Tb multilayer [20]. Earlier, Fe layers in Fe/Tb multilayers have been shown to become amorphous for a thickness of 0.5–1.5 nm, accompanied by a change from ferromagnetic to superparamagnetic behavior [21]. This was due to clustering at the interface of very thin layers. The magnetic behavior of the present Fe/Tb system, however, is that of a normal ferromagnetic system plausibly due to the thickness of the Fe layer (~3.0 nm). The high-field spontaneous magnetization are responsible for an increase in their values (up to certain fields of measurements <10 kOe) with increase in temperatures. The FC-ZFC furcation points (T_F) are at much lower temperatures (25–100 K) when compared with the bulk and thin film Tb samples. Such an effect may be due to changes in thickness of the Tb layer affecting the morphology of the layers in the heterostructure. Note that there is a net magnetization even at 300 K which remains similar with fields below 10 kOe and decreases only above 70 kOe. This decrease is not clearly understood at present.

2. Magnetic hysteresis

The temperature dependence of the hysteresis loops for $[Fe/Tb]_5$ is shown in Fig. 3 after field cooling. The loop measured at 10 K was conducted at 70 kOe, while for all other measurements a field of 50 kOe was applied. The most

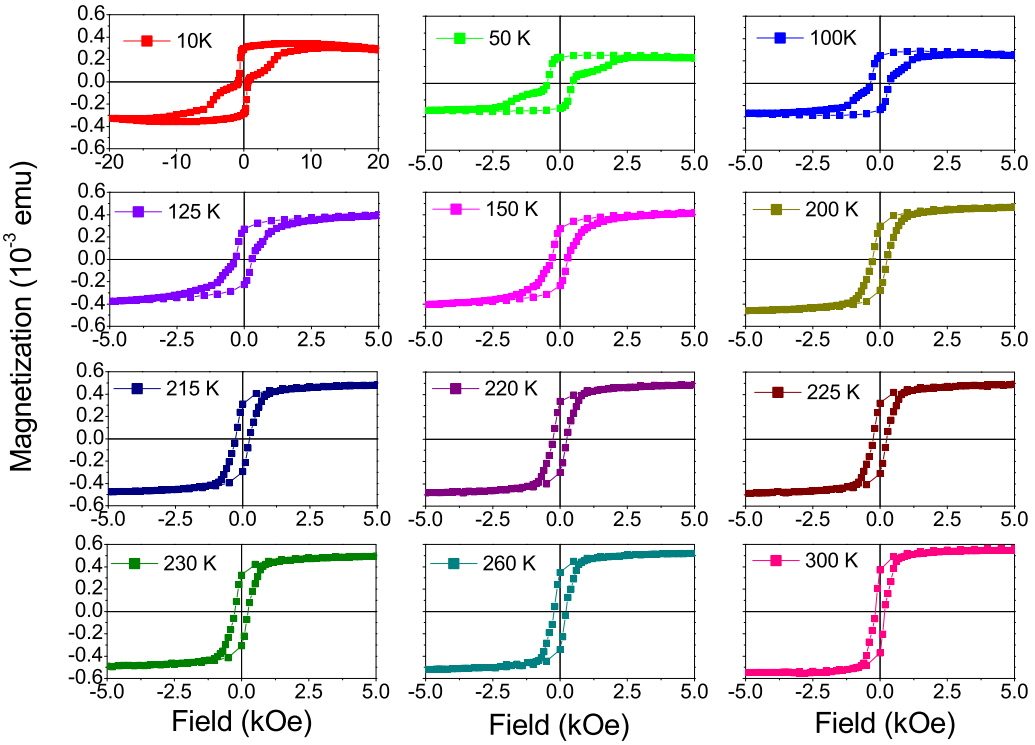

FIG. 3. (Color online) Hysteresis loops for $[Fe/Tb]_{\times N=5}$ sample at various temperatures after field cooling in 50 kOe from 300 K. The loops are corrected for their diamagnetic contributions.

interesting aspect, however, is evident at and below 150 K. Here, a secondary loop (bottom half) evolves that is shifted opposite to the field cooling axis (negative shift), i.e., along the decreasing branch of the hysteresis loop. This type of shifts are typical for an exchange coupled AF-FM system, where the uncompensated moments in the AF are coupled with the FM moments. However, we could see a similar shift (top half) along the increasing branch of the same loop as well. One may note that we did not find any such shift and no coupling for a simple bilayer [Fe/Tb] using the same field and temperature histories. We therefore categorize the hysteresis loops in terms of a superimposition of two loops. The first one is called the primary loop, which has its center at 0.0 Oe along the x axis. The second one is called the secondary loop, which has its center shifted horizontally along the x axis, in the positive and negative field directions.

Such a superposition of two secondary loops has been reported earlier and was named "double hysteresis loop" (DHL) [22]. Such DHLs are, however, a result of intermediate cooling fields for non saturated FMs. In this case, the AF is broken into a bidomain state, i.e., oppositely biased subsystems with equal magnitudes of exchange bias acting on the FM. This is possible if the AF domain size is much larger than the FM domain size. For our Fe/Tb sample, the DHLs are also symmetric and have almost equal H_c values. In contrast to Ref. [22], however, we applied a much larger cooling field, i.e., much beyond the saturation value of 5 kOe of the system.

The horizontal shifts are defined by the exchange bias $H_{eb} = (H_c^{+\alpha} + H_c^{-\alpha})/2$ and the coercive fields $H_c = (H_c^{+\alpha} - H_c^{-\alpha})/2$, where $H_c^{+\alpha/-\alpha}$ are the coercive fields for the positive and negative field axes. Here, $\alpha = p/s$ depending upon the values from the primary (p) or secondary (s) loops. Figure 4(a) shows the respective coercive fields for a representative double-loop character of the hysteresis when measured at 50 K. The temperature dependence of H_c and H_{eb} of $[Fe/Tb]_5$ is shown in Fig. 4(b). The shifts in the two secondary loops are regarded as anomalous since the coercivity is seen to increase up to 2 kOe at 10 K which is significantly higher than for a conventional AF-FM coupled system [23]. Note that TM-RE

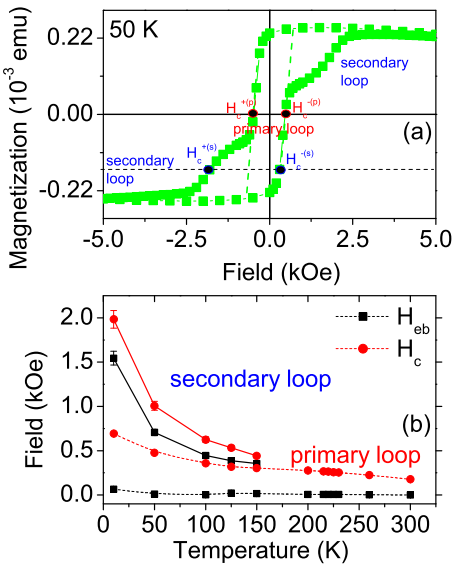

FIG. 4. (Color online) (a) Representative hysteresis loop at 50 K showing the coercivities of the primary and secondary loops. (b) Temperature dependence of H_c and H_{eb} for $[Fe/Tb]_5$ from the primary and secondary loops.

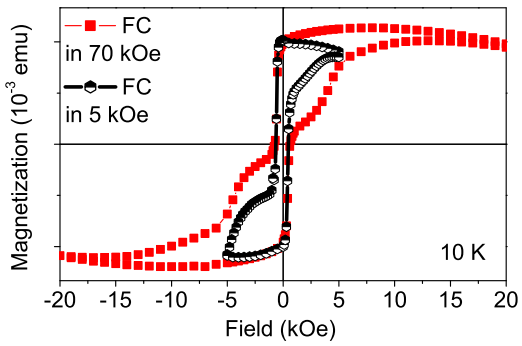

FIG. 5. (Color online) Hysteresis loops for $[Fe/Tb]_5$ at 10 K after field cooling from 300 K in 70 and 5 kOe.

alloy systems like GdFe/TbFe show much lower coercive fields (∼0.05 kOe) [8]. Therefore the exchange coupling between the Tb and Fe layers in $[Fe/Tb]_5$ is very strong.

Generally, when the coupling at the interface between the net magnetization of the two layers is antiferromagnetic, it leads to a positive exchange bias shift and when the coupling is ferromagnetic, the shift is negative. The fact that we observe a negative shift for the bottom half of the hysteresis loop along the decreasing branch, apparently indicates of a ferromagnetic alignment of the Fe and Tb moments upon field cooling below the blocking temperature of the Tb layer. The observation of a similar shift for the top half of the hysteresis loop along the increasing branch indicates of a realignment of the moments along the anisotropy axis in the direction opposite to the field cooled state after saturation along the opposite branch, as predicted for a bidomain state of the AF.

The loops are showing symmetric shifts along the decreasing as well as along the increasing branch of the loop. This can be ascribed to a situation where the AF domains remain larger (restricted by anisotropy) than their FM counterparts and behave like a bidomainlike state. This is evident by comparing the minor hysteresis loop with the major loop measured at 10 K as shown in Fig. 5. Here, the sample was cooled in $H = 5$ kOe from 300 K instead of 70 kOe. The field loops were restricted to ±5 kOe (instead of ±70 kOe). It is evident from the data that the secondary loop along the increasing branch is less prominent with lowering of the cooling field indicating a bidomainlike state. Note that for a bidomainlike state in a low cooling field, one observes a negative shift while for a high cooling field, higher than for the destruction of AF order, one observes a positive shift but for intermediate cooling fields one only observes DHLs [22]. In our case, due to the intermediate cooling field, the system is divided into two spatially separated proportions or subsystems, the Fe moments for one of which are coupled to the Tb moments in one direction and for the other proportion they remain oppositely coupled and this coupling varies with temperature and cooling field. A bidomainlike state is more likely to form, for example, in FeF_2 layers, due to intrinsic pseudotwin domains in the AF [22]. In case of Tb, however, Cornor *et al.* reported of 180° Bloch walls (few tens of micrometers) in the basal plane separating the domains magnetized alternately parallel and antiparallel to the *b* direction [24].

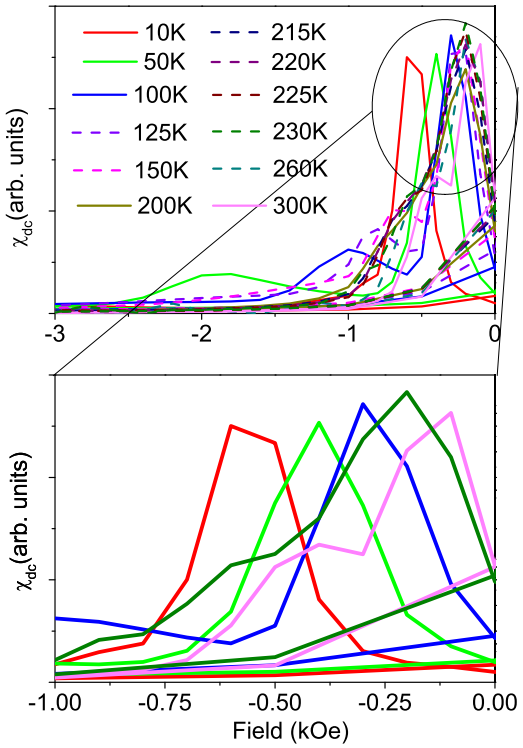

FIG. 6. (Color online) $\chi_{dc}(=dM/dH)$ is shown as a function of temperature for $[Fe/Tb]_5$. The bottom panel shows an enlargement of the data at low fields.

3. *Direct-current susceptibility*

The dc susceptibility $\chi_{dc} = \frac{dM}{dH}$ for $[Fe/Tb]_5$ is shown in Fig. 6. χ_{dc} shows clearly two peaks (first/second one is below/above 0.8 kOe) at the temperatures where the slope of the magnetization shows reversal points. The effect is particularly clear at low temperatures. We find distinct and gradual shifts for both reversal fields with lowering of the temperature. The first peak shift is relatively much smaller (by an order of magnitude) than the second and is typical of weakly coupled FM layer. No frequency dependence is found for ac fields with a frequency up to 10 kHz indicating a coupling of all the Fe and Tb layers.

C. Polarized neutron reflectivity measurements: Fe/Tb multilayer

Specular and off-specular reflectivity measurements were performed using the reflectometer TREFF at FRM II. The scattering geometry is shown in Fig. 7. The sample surface defines the x-y plane. The z axis is perpendicular to the surface normal. The momentum transfers along the z and x directions are given by

$$\vec{Q}_z = \frac{2\pi}{\lambda}[\sin(\alpha_i) + \sin(\alpha_f)], \quad (1)$$

and

$$\vec{Q}_x = \frac{2\pi}{\lambda}[\cos(\alpha_f) - \cos(\alpha_i)], \quad (2)$$

respectively. Off-specular scattering contributions along $\vec{Q}_x$ arise if the in-plane translational symmetry is broken by

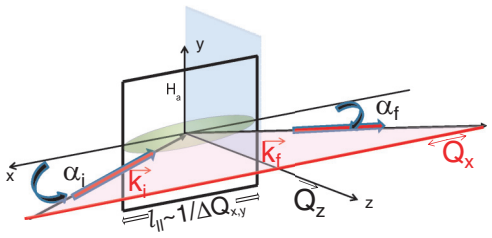

FIG. 7. (Color online) Schematic of the neutron scattering geometry at TREFF. $\mathbf{k}_i$ and $\mathbf{k}_f$ designate the wave vectors of the incident and scattered neutrons, respectively. The z direction is defined to be perpendicular to the film plane.

interface roughness or by magnetic domains on a length scale shorter than the in-plane projection of the neutron coherence length $l_\parallel$ [25]. For TREFF, we obtain $l_x \approx \frac{\lambda}{\alpha_i \Delta\alpha_i} \sim 25\ \mu$m for $\alpha_i = 20$ mrad and an uncertainty $\Delta\alpha_i = 1$ mrad. The lack of any off-specular scattering from our sample indicates that the lateral dimension of the magnetic or structural correlations are either larger than l_x or much smaller than a micron.

In the present experimental geometry, only $\vec{Q}_x$ is resolved whereas the scattering is integrated along Q_y due to the relaxed collimation along the y direction. The reflectivity is given by the superposition of the nuclear and magnetic scattering length densities of the film, i.e., ρ_n and ρ_m. Components of ρ_m parallel/antiparallel to the neutron polarization are added/subtracted from ρ_n giving rise to non-spin-flip (NSF) scattering, i.e., $\rho_n \pm \rho_m \cos\phi_A$ represented by R_{++} and R_{--}. The spin-flip (SF) scattering, given by $\rho_m^2 \sin^2\phi_A$, is represented by R_{+-} and R_{-+}. Here, ϕ_A is the angle between the magnetization $\mathbf{M}$ and the applied field $\mathbf{H}_a$. By analyzing the polarization of the reflected neutrons, it is possible to resolve the components of the in plane magnetization along the x and y directions.

Typical reflectivity profiles R_{--} and R_{++} measured at 300 K in an external field $H_a = -4$ kOe are shown in Fig. 8. Before the measurement, the sample was saturated in a field $H_a = +5$ kOe. Clearly visible are two superlattice peaks at the Q_z positions given by 2π times the inverse of the bilayer thickness of the $[Fe/Tb]_5$ multilayer. According to these data, we explain how we analyzed the field and temperature dependencies of the reflectivity data shown below.

1. Model fitting

In order to confirm the structure of the multilayer, we have first fitted x-ray reflectivity profiles (not shown) using a model based on the as made multilayer. The fits show that the thickness of the layers are close to their nominal values with an error bar of ± 0.2 nm. The interface roughness is $\simeq 0.5 \pm 0.2$ nm. The obtained scattering length densities are $\rho_{Tb} = 4.8 \pm 0.2 \times 10^{-5}$ Å^{-2} and $\rho_{Fe} = 5.4 \pm 0.2 \times 10^{-5}$ Å^{-2}, respectively.

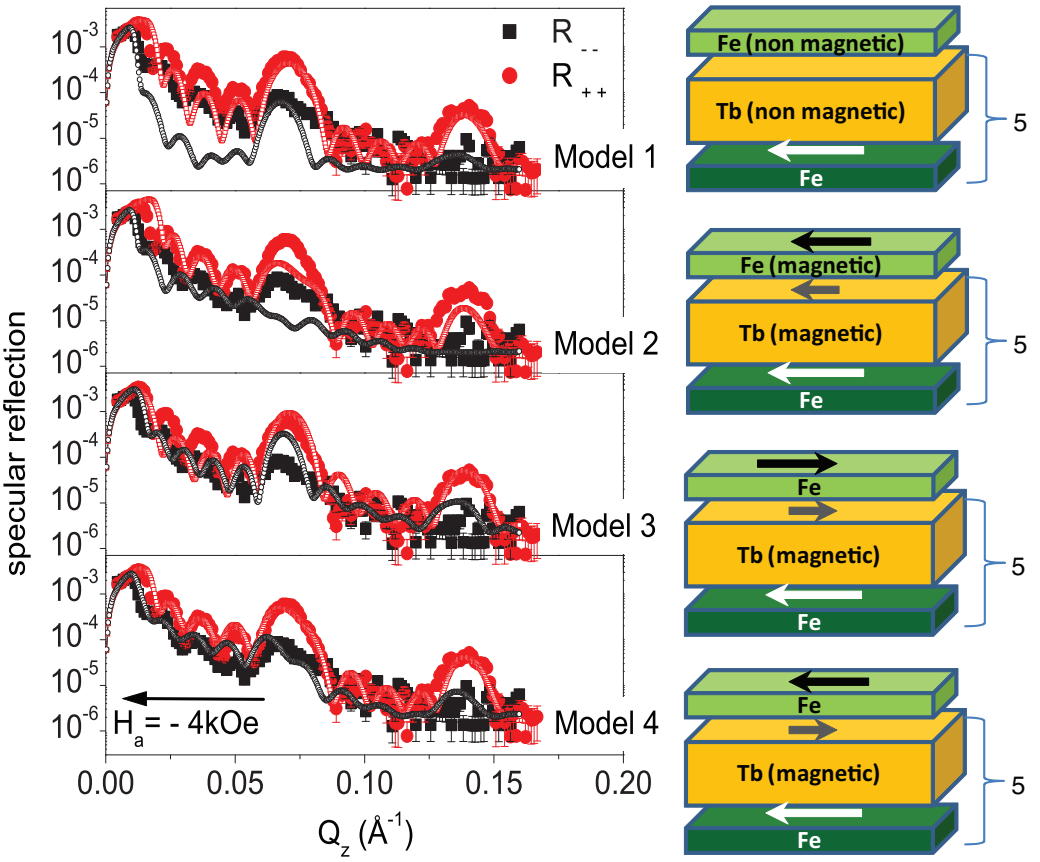

FIG. 8. (Color online) (a)–(d) Reflectivity profiles measured at 300 K in a field $H_a = -4$ kOe along the decreasing branch of the hysteresis loop are shown on the left-hand side. The open symbols show fits based on the models described in the text. Schematics of each of the models considered are also given alongside.

To determine the magnetic structure of the multilayer, we have assumed four models that are listed in a chronological order (Fig. 8). Note that the sample is at $H_a = -4$ kOe in saturation, i.e., the saturation moments can be determined. The parameters used for fitting the 300-K data at saturation were the thickness and the SLD parameters (shown within a later figure) of individual layers within a stack of five bilayers. The interface roughness was kept at $\simeq 0.5 \pm 0.2$ nm. We do not consider any intermixed layer at the interface of Fe and Tb layers. The fits yield the following values for the scattering densities: $\rho_{\rm n}^{\rm Tb} = 3.0 \pm 0.2 \times 10^{-6}$ Å^{-2}, $\rho_{\rm m}^{\rm Tb} = 1.0 \pm 0.1 \times 10^{-6}$ Å^{-2}, $\rho_{n}^{\rm Fe} = 5.0 \pm 0.2 \times 10^{-6}$ Å^{-2}, and $\rho_{m}^{\rm Fe} = 4.5 \pm 0.1 \times 10^{-6}$ Å^{-2}. The magnetic scattering length density of the top Fe layer was fitted independently from the stack. As the top Fe layer may be slightly oxidized, we assumed a reduced nuclear scattering length density 2.0×10^{-6} Å^{-2} when compared with the stack $\approx 5.0 \times 10^{-6}$ Å^{-2}. Fitted parameters were obtained using the minimization of χ^2 (or the goodness of fit) for each model. The errors in the thickness of the layers are ± 0.2 nm, while that for the ρ_n and ρ_m values are $\pm 0.2 \times 10^{-6}$ and $\pm 0.1 \times 10^{-6}$ Å^{-2}, respectively.

(1) Following the magnetic phase diagram for thin film Tb we assume a moment $\mu_{\rm Tb} = 0$. The top Fe layer is assumed in this model to be nonmagnetic. Clearly, model 1 cannot explain the data. (2) In this model, we assume that Tb has a magnetic moment and this magnetic moment is parallel to the Fe moments in the stack. We also consider the top Fe layer to be magnetic and has the same direction as that of the stack. Again, there is a strong disagreement with the data. (3) Coupling at two FM interfaces, separated by an AF, can be quite different as has been observed in bilayer and trilayered samples [26]. Next, we therefore consider the top Fe layer, which is not sandwiched between two Tb layers and is FM-coupled to the adjacent Tb layer (alternatively, a FM-coupled layer at the bottom and FM-coupled top and bottom layers were also considered). The remaining five Fe layers are coupled antiferromagnetically to the Tb layers. A better agreement is obtained with the data as compared to model 2, though not satisfactory. (4) Finally, an antiferromagnetic coupling between all Tb and Fe layers is assumed, i.e., the Tb and Fe moments in the stack are always antiparallel. This leads to a very good agreement with the data. The coupling strength between the Fe and the Tb layer does not become altered if the Fe layer is sandwiched between two Tb layers or is interfaced with a single Tb layer, only the lowest equilibrium configuration at a given magnetic field might become altered. In the following, we have always used model 4 as a starting point in the process of fitting the data, i.e., an antiferromagnetic coupling between the Tb and Fe layers composing the bilayers and a ferromagnetic coupling between the Tb and the top Fe layer.

2. *Reflectivity data*

Figures 9(a) and 9(d) display specular PNR data measured at 300 K for various applied fields $H_{\rm a}$. First, the sample was saturated in a field of 5 kOe followed by PNR measurements in an increasing negative field. Around the coercive field $H_a = -0.17$ kOe, a crossing of the R_{++} and R_{--} channels occurs indicating a reversal of the magnetization of the system. Note that all the layers undergo a simultaneous π reversal,

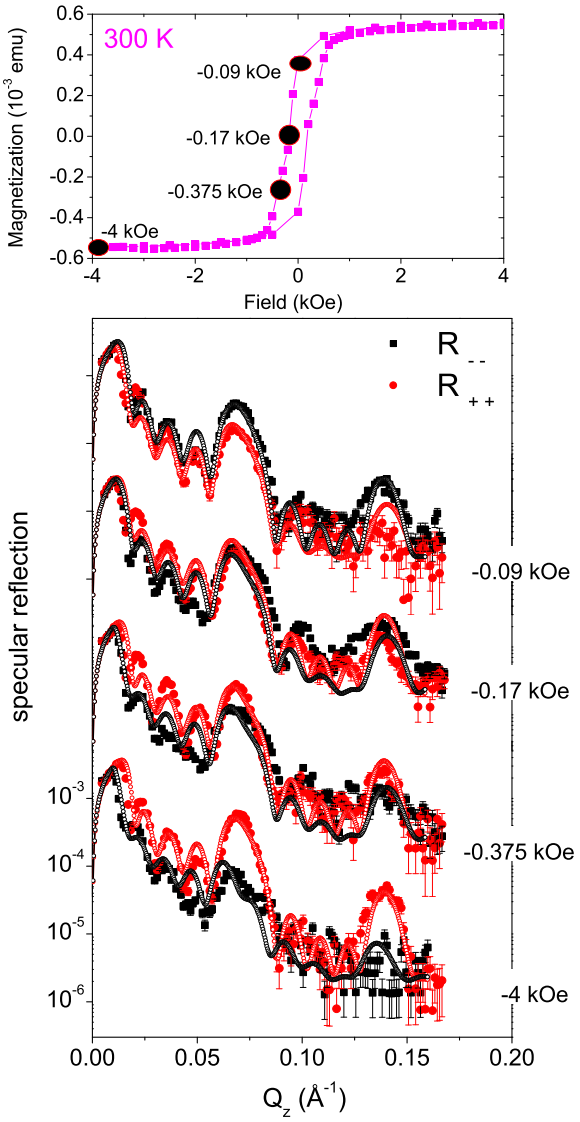

FIG. 9. (Color online) (a)–(d) PNR measurements at 300 K for spin-up and spin-down polarizations for various applied fields $H_{\rm a}$ along the decreasing branch of the hysteresis loop are plotted versus $\vec{Q}_z$ along with their best fits (open symbols). The top panel shows the corresponding hysteresis loop. The field values for the neutron measurements are marked as circles in the top panel.

i.e., there is no successive flipping of layers. In particular, the magnetization of the AF-coupled Tb layer also undergoes a reversal at the same field.

Figures 10(a)–10(d) display specular PNR data measured at 50 K for various $H_{\rm a}$. The sample was first saturated in a field of 5 kOe before the measurements were started at –0.09 kOe and onwards. Clearly, the magnetization completes its reversal (crossing of R_{++} and R_{--}) around –1.4 kOe being consistent with the shift of the loop seen in the SQUID data (top panel of Fig. 10). The complete π flip of all the layers occurs only at the secondary coercive field $H_{\rm c}^{-s} = -1.4$ kOe. At the primary field $H_{\rm c}^{-p} = -0.375$ kOe only a partial rotation of domains has taken place along the field direction which cannot be clearly inferred from the NSF data alone. Note that such a distinction between $H_{\rm c}^{-p}$ and $H_{\rm c}^{-s}$ was not possible at 300 K as only a

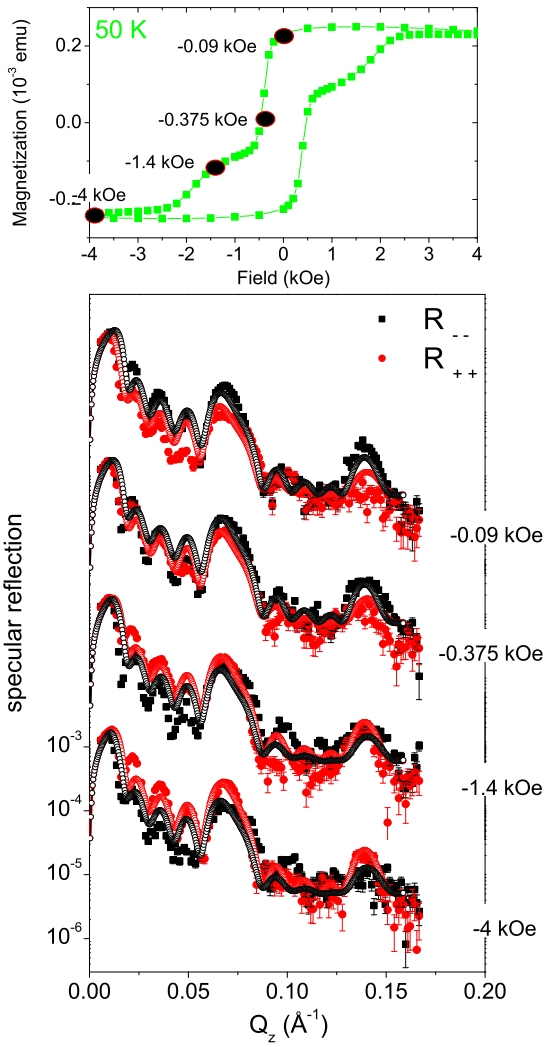

FIG. 10. (Color online) (a)–(d) PNR curves at 50 K for spin-up and spin-down polarizations measured at various applied fields H_a along the decreasing branch of the hysteresis loop are plotted versus $\vec{Q}_z$ along with their best fits (open symbols). The top panel shows the corresponding hysteresis loop. The field values for neutron measurements are indicated alongside (marked in circles in the top panel) in both panels.

small change of slope is observed in the hysteresis loop (top panel of Fig. 9). Measurements at even lower temperatures could not be conducted due to the lack of a high field magnet with $H > 20$ kOe.

3. *Analysis of reflectivity data*

To analyze the data in more detail, we have fitted the reflectivity data assuming the parameters of model 4 for the measurements at 300 and 50 K. The parameters that were used for fitting the temperature and field dependent data are the magnetic SLDs of the individual layers. In particular, we have assumed that the magnetic coupling between the Fe and the Tb layers (FM and AF) does not change with temperature. Figures 11(a) and 11(b) show the depth dependence of the nuclear (ρ_n) and magnetic (ρ_m) scattering length densities for $T = 300$ and 50 K as measured at saturation. With increasing

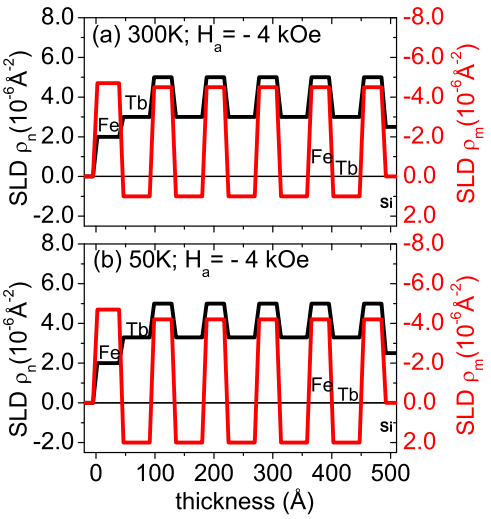

FIG. 11. (Color online) The nuclear (ρ_n) and magnetic (ρ_m) SLDs vs the thickness of the multilayer are shown for 300 and 50 K at saturation $H_a = -4$ kOe after saturating the sample in +5 kOe.

T, the magnetization in the Tb layers is significantly reduced which can be due to its magnetic phase changes, while there is a small decrease in the Fe layer magnetization. The data confirm the increase of the Tb saturation moment by almost a factor of two when cooling from 300 to 50 K, namely from $1.4 \pm 0.2\mu_B$/atom to $2.4 \pm 0.2\mu_B$/atom. Clearly, Tb is magnetically ordered even at 300 K. In contrast, the Fe saturation moment decreases from $2.0 \pm 0.2\mu_B$/atom at 300 K to $1.8 \pm 0.2\mu_B$/atom at 50 K. This is lower than the experimentally determined magnetic moment of 2.2 μ_B/atom for Fe [27], which indicates of a DW formation in our case.

Figure 12 shows the field dependence of ρ_m. It is clearly seen that the magnetization changes sign at a much higher field at 50 K than at 300 K, i.e., the coercive fields are distinctly different. With decreasing T the exchange coupling between the Tb and Fe layers increases, an effect that is most likely associated with the evolving helical phase in Tb which appears at much lower T than in the bulk or in thick films.

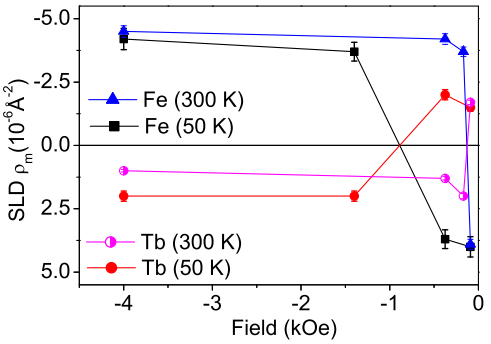

FIG. 12. (Color online) The field dependence of ρ_m for the Fe and Tb layers is shown at 300 K and 50 K. Before the experiment, the multilayer was saturated in a field $H_a = +5$ kOe.

4. Discussion

Similar DHL were observed by Kim *et al.* [2] on perpendicularly anisotropic Fe/Tb multilayers. They were explained in terms of loops from a typical ferromagnet with two subsystems and hence two H_c's from the lower and upper interfaces. In our system, we can rule out the formation of such distinct subsystems. This is primarily due to the fact that here we have only five bilayers instead of 20 or more where more number of layers increase the possibility of two subsystems.

Similarly looking DHLs were also observed earlier in CoNi/Gd/CoNi trilayer systems [10]. On cooling, these loops shifted opposite/along the cooling field depending upon the magnetization of the RE layer with respect to the FM layers. They observed DHLs in decoupled trilayer systems (where a thicker RE layer decoupled the two FM layers on either side) with Gd layer thickness of more than 8 nm. The difference in coercivities that were evident clearly at 300 K for the Gd based trilayer, gradually disappeared at field cooled states to form either negative or positive loop shifts. The present hysteresis loops, even though apparently may indicate a similar case of different coercivities of the subsystem, actually depicts a significantly different situation. One may note that the thickness of the Tb layer, in the present case, is only ∼6 nm and the system is not decoupled at 300 K. One should also note that the existence of a hard ferrimagnetic RE alloy at the interface that was attributed to the formation of a ferrimagnetic system, resulting in different coercivities of the Gd alloy and CoNi subsystems, does not exist here. In our case, Fe-Tb has positive heat of mixing (causing demixing at the interfaces not allowing alloy formation) [3], and we do not see any loop shift nor the DHLs at 300 K but only at field cooled states below ∼150 K. Thus we can also rule out such possibility of subsystems to coexist in our multilayer.

The two coercivities that we see in the multilayer are probably due to the top and/or bottom Fe layer hysteresis $H_c^{\pm p}$'s (primary) [26] superimposed on the DHLs $H_c^{\pm s}$'s (secondary) of the rest of the stack. The rest of the stack have almost similar switching fields close to that of the secondary loop switching. This was also evident from the small temperature evolution (from ≈−0.12 kOe at 300 K to −0.55 kOe at 10 K) of the primary loop H_c^{-p} as compared to the large evolution (from ≈−0.4 kOe at 300 K to −4.5 kOe at 10 K) of the secondary loop H_c^{-s} (Fig. 4). In case they were from two subsystems—coupled to each other—their evolution with temperature would have been very similar in magnitude.

The most definite proof of the DHLs follows from our detailed simulations of the PNR data at various fields and at various temperatures. We did not find any signature of layer-by-layer flipping at any measuring field, which is expected in case of layers with different switching fields from top to bottom or due to layers with different anisotropies within the layer stack. In our case, all layers in the five layers stack switch simultaneously and the reversal mechanism involved is strictly via a domain nucleation process. To demonstrate this aspect further, we concentrate on the 50 K data measured at −1.4 kOe. One should note that PNR is highly sensitive to the orientation of the layer magnetization with respect to the applied field direction and the data covers a relatively large $\vec{Q}$ range. Note that it is exactly the same model (model4) which was described earlier has been used for fitting the PNR data. Note also that the coercive field or the reversal point (crossing point of R_{++} and R_{--}) has shifted from −0.17 kOe at 300 K to −1.4 kOe at 50 K. This clearly signifies the shift of the loop with temperature along the field axis and thereby the sensitivity of the PNR data as it follows the hysteresis loop at two different temperatures. The simulated data in Fig. 13 clearly shows the large degree of discrepancies from the measurements as we consider 1, 2, and

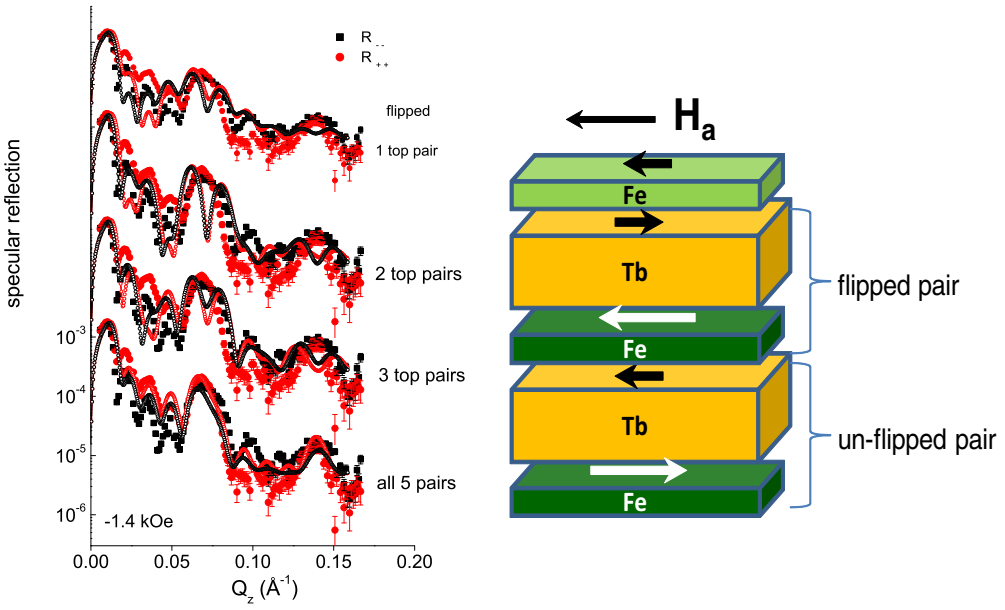

FIG. 13. (Color online) PNR profiles measured at 50 K in a field of $H_a = -1.4$ kOe along the decreasing branch of the hysteresis loop are shown along with the simulations (open symbols). The simulations are done using model 4 and considering 1, 2, 3, and 5 layer pairs of AF-coupled Fe and Tb layers in the stack to flip as shown in the schematic alongside. The simulations are shown to support the case of simultaneous flipping of the layers against layer-by-layer flipping.

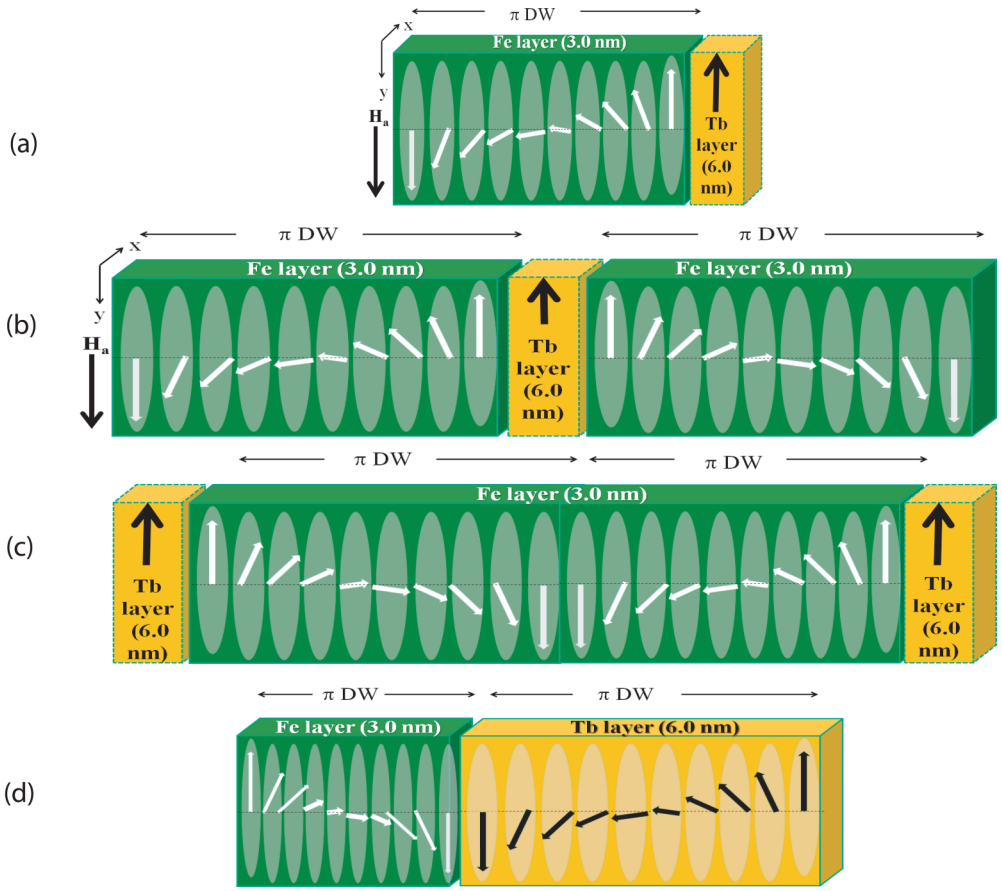

FIG. 14. (Color online) Schematic of (a) π-DW propagation in a Fe layer against an anisotropic Tb layer (b) 2π-DW propagation against an anisotropic Tb layer sandwiched between two Fe layers (c) 2π-DW propagation in a sandwiched Fe layer against two anisotropic Tb layers and (d) 2π-DW propagation through the Fe and Tb layers. The thickness of the Fe layer is often exaggerated as compared to the Tb layer thickness to better show the evolvement of the DW.

3 of the top pairs of (AF coupled) Fe and Tb layers to flip. The fits are in agreement with the data only when we consider all the five Fe-Tb layer pairs have flipped. The simultaneous flipping of layers in the stack, instead of layer-by-layer flipping, thus rules out the existence of subsystems with different coercivities in the stack of five bilayers.

It is well known that moments of magnetic 3*d* elements couple antiferromagnetically to the moments of RE elements [28] and also that RE in contact with Fe develops an induced moment even at RT [29]. These two previous observations are in absolute agreement with our present observations. The magnetic moments of Tb at 300 K is a result of such induced magnetization from the Fe proximity. The 3*d*-5*d* hybridization not only produces significant 5*d* density at the RE-sites but is also responsible for the crucial coupling between the RE and TM moments. The essential point to realize is that the RE-4*f* and RE-5*d* spins are coupled by local exchange interactions (which are essentially ferromagnetic) and that the interaction between RE-4*f* and TM-3*d* spins is mediated entirely by the RE-5*d* TM-3*d* hybridization [30]. Thus a Tb layer sandwiched between two Fe layers always maintain an antiferromagnetic order with an Fe layer.

A more intrinsic requirement of an exchange bias is not necessarily a ferro-antiferromagnetic interface. The EB may also occur due to the development of a DW at the interface that does not respond to an external field. This can be realized if, e.g., the net magnetization is zero as in an AF or in a material with very strong anisotropy as in a RE. The exchange bias like behavior in our samples is a result of such DWs at the interface. Actually, it was proposed for other combinations of Fe/RE bilayers that the Fe layer can developed a 180°–DW at the interface [8]. As Fe is the softer material, it is expected that the nucleation of the DW takes place within the Fe layers, because the magnetization of the Tb layer is constrained by its strong anisotropy [9]. In case the Tb layer was an AF layer, the DWs would have tend to propagate from one Fe layer to the other Fe layer. In the present case, they are blocked on their way as they are compressed against the Tb layer. However, due to the presence of the Tb layer on both sides of each Fe layer, it is more likely that the DW propagates via 2π-DWs instead of π-DWs, commonly observed at hard-soft (RE-TM) bilayer (or TM-RE-TM trilayer) interfaces as explained next.

We show a schematic of the possible scenarios of 2π-DW propagation in our Fe/Tb multilayer as compared to π-DW propagation in a Fe/Tb bilayer or in trilayer in Fig. 14. The situations sketched are (a) π-DW propagation in a Fe layer against an anisotropic Tb layer, (b) 2π-DW propagation against an anisotropic Tb layer sandwiched between two Fe layers, (c) 2π-DW propagation in a sandwiched Fe layer

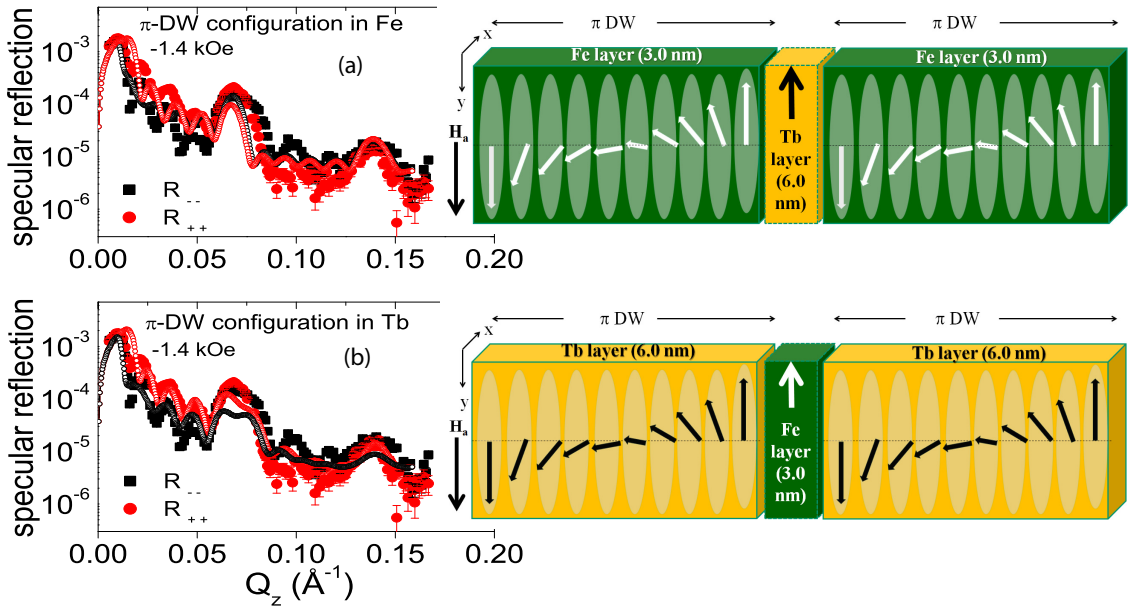

FIG. 15. (Color online) PNR profiles measured at 50 K in a field of $H_a = -1.4$ kOe along the decreasing branch of the hysteresis loop are shown along with the simulations (open symbols) considering π-DW propagation (a) within the Fe layers against anisotropic Tb layers or (b) within the Tb layers across thin Fe layers. Shown alongside are the schematics of the π-DW propagations.

against two anisotropic Tb layers, and (d) 2π-DW propagation through a Fe and also through a Tb layer. The thickness of the Fe layer is often exaggerated compared to the Tb layer thickness to better show the evolvement of the DW. To understand the mechanism in more detail, we concentrate on the hysteresis loop at 50 K where clearly two hysteresis loops are observed. The decrease of magnetization around the primary loop indicates the beginning of nucleation of reverse magnetization within Fe (decrease in ρ_m). The magnetization decreases slowly between -0.375 to -1.4 kOe. Around -1.4 kOe, the DWs propagate through the Tb layer as the magnetizations of the Tb layers reverse, which give rise to a second nucleation. Beyond this field, the DW in Fe is fully compressed. It decompresses and compresses similarly along its reverse path.

To explore the possible existence of π-DWs in the system, we simulate the PNR spectra corresponding to the 50 K data measured at -1.4 kOe. Here, at this field, the probability of DWs to exist is high. The parameters (thickness, roughness and nuclear SLDs) of each layer are kept the same used for fitting the data considering single domain layers with which reasonable agreement was achieved. The simulated spectra in Fig. 15(a), assuming DWS to spread in the softer Fe layers, has been shown. The Fe layer has been divided into 10 sublayers ($i = 1$–10) each one of which is $\approx$0.3-nm thick. The magnetic SLDs of each layer is proportional to cos θ, which exhibit an angle $\theta(i)$ with respect to the applied field $\mathbf{H}_a$. We assume $\theta(i = 1)$=0 for the bottom and $\theta(i = 10)$=π at the interface with Tb (i.e., along the Tb moment direction). Thus a DW width of $\sim$3.0 nm is obtained. In Fig. 15(b), we show a similar simulation considering π-DWs to propagate within the Tb layers instead of within the Fe layers. The magnetic configurations corresponding to cos θ of each sublayer is plotted schematically alongside. We find large discrepancies as we compare the simulated spectra with the experimental data. One should compare these simulations with the fits considering no DWs that are shown in Fig. 10. Thus PNR confirms that no π-DWs exist in the system. On similar treatment with 2π-DWs it is not possible to discern between their existence and non existence particularly due to the small thickness of the FM layers. In fact, this is quite complicate to simulate DWs in a multilayer as their widths can can vary from layer to layer and even can spread in both layers and may exist with different proportions of extensions and compressions in each layer.

Following Mangin *et al.* [9], we consider a infinite linear chain of Fe spins, which propagate along the x direction. In a field $\mathbf{H}_a$ applied along the easy axis, the magnetization at the position x will exhibit an angle $\theta(x)$ with respect to $\mathbf{H}_a$. The exchange energy due to the presence of a 2π-DW is given by

$$E = \int_{-\infty}^{+\infty} \left\{ A\left(\frac{d\theta}{dx}\right)^2 + M_{\mathrm{FM}} H_a [1 - \cos\theta(x)] + K_{\mathrm{FM}} \sin^2\theta(x) \right\} dx. \quad (3)$$

The boundary conditions are $\theta(-\infty) = 0$ and $\theta(+\infty) = 2\pi$. Here, $A = 2 \times 10^{-7}$ erg/cm [31] is the exchange constant and $K_{\mathrm{FM}} = 4.4 \times 10^3$ erg/cm^3 [32,33] is the uniaxial anisotropy of the Fe layer. This expression, on energy minimization and as θ approaches 2π, provides an estimate of the DW thickness of $\approx$27 nm at around -0.1 kOe and $\approx$7 nm at around -1.4 kOe. These magnitudes are of the same order as the thickness of the Fe layers, which is around 3 nm ($\sim$15 monolayers). A similar interfacial domain wall thickness $d = 3$–4 nm was found in other Fe-Tb based systems with AF coupling [34]. Thus we can predict such DW formations in our Fe/Tb system, even though there is no direct evidence. In this regard, one may note that the extent of DWs (of few tens of nanometers) that are possible in other bilayer RE-TM systems are where the FM layer thicknesses range around hundreds of nanometers [8]. Such

large domains are not possible to form in our multilayers as the individual thicknesses do not extend over few nanometers. Therefore we believe that the extent of nanometric 2π-DWs in our RE-TM multilayer can only explain the origin of the exchange bias.

IV. SUMMARY

We have studied the exchange coupling in $[Fe/Tb]_5$ multilayers after field cooling the system in 50 kOe from 300 to 2 K. The magnetization was measured in an in-plane applied field along the decreasing branch of the hysteresis loop. Below 150 K, the formation of a (i) double hysteresis loop (DHL) associated with (ii) exchange-bias-like loop shifts along and opposite to the field cooling axis is observed. The maximum H_{eb} for the DHLs is of the order of 1.54 kOe.

PNR measurements on $[Fe/Tb]_5$ were performed at 50 and 300 K for various fields H_a. The fits of the PNR curves confirm the antiferromagnetic alignment of the Fe and Tb layers leading to a ferrimagnetic alignment of the Fe and the Tb layers. The temperature evolution of the coercivities do not indicate of a decoupled system showing the DHLs which is also corroborated by the PNR data and model simulations. The DHLs are explained by the formation of bidomainlike states in the Tb layers similar to that in AF systems. The main difference from a typical AF-FM system is that the anisotropically hard Tb layers in the Fe/Tb multilayer forming these bidomains, posses a significant magnetic moment. They form oppositely biased subsystems with equal magnitudes of exchange bias acting on the softer Fe layer. We demonstrate the appearance of an induced magnetic moment in the ≈6.0-nm Tb layer even at 300 K for this ferrimagnetic multilayer. Moreover, the evolution of the magnetic structure with temperature clearly indicates the increase of the exchange coupling at the Fe/Tb interface with decreasing T. The possible formation of 2π-DWs within the Fe layers blocked by the anisotropic Tb layers can be attributed to the exchange bias. The formation of π domain walls is excluded.

ACKNOWLEDGMENTS

We would like to thank S. Mattauch and Andreas Ofner for granting beam time at TREFF and M. Opel for allowing to use the SQUID magnetometer. We would also like to thank J. Mannhart, A. Herrnberger, T. Mairoser, and A. Schmehl for the collaboration during the course of realizing the sample deposition chamber at the University of Augsburg for the Transregional Collaborative Research Center TRR 80 of the Deutsche Forschungsgemeinschaft.

[1] T. Morishita, Y. Togami, and K. Tsushima, J. Phys. Soc. Jpn. **54**, 37 (1985).
[2] W. S. Kim, W. Andrä, and W. Kleemann, Phys. Rev. B **58**, 6346 (1998); W. S. Kim, W. Kleemann, J. Tappert, and W. Keune, J. Appl. Phys. **84**, 4384 (1998).
[3] A. Gupta, A. Paul, R. Gupta, D. K. Avasthi, and G. Principi, J. Phys. Condens. Matter **10**, 9669 (1998).
[4] W. H. Meiklejohn and C. P. Bean, Phys. Rev. **102**, 1413 (1956).
[5] A. Paul, Pramana J. Phys. **78(1)**, 1 (2012).
[6] J. Nogués, D. Lederman, T. J. Moran, and Ivan K. Schuller, Phys. Rev. Lett. **76**, 4624 (1996).
[7] T. L. Kirk, O. Hellwig, and E. E. Fullerton, Phys. Rev. B **65**, 224426 (2002).
[8] F. Canet, C. Bellouard, S. Mangin, C. Chatelain, C. Senet, R. Siebrecht, V. Leiner, and M. Piecuch, Eur. Phys. J. **34**, 381 (2003).
[9] S. Mangin, G. Marchal, and B. Barbara, Phys. Rev. Lett. **82**, 4336 (1999).
[10] B. Altuncevahir and A. R. Koymen, J. Magn. Magn. Mater. **261**, 424 (2003).
[11] D. J. Webb, A. F. Marshall, Z. Sun, T. H. Geballe, and R. M. White, IEEE Trans. Magn. **24**, 588 (1988).
[12] F. Hellmann, R. B. van Dover, and E. M. Gyorgy, Appl. Phys. Lett. **50**, 296 (1987).
[13] S. Mangin, F. Montaigne, and A. Schuhl, Phys. Rev. B **68**, 140404 (2003).
[14] A. V. Svalov, V. O. Vas'kovskiy, N. N. Schegoleva, and G. V. Kurlyandskaya, Tech. Phys. **50**, 914 (2005).
[15] J. J. Hauser, Solid State Commun. **55**, 163 (1985); C. Y. Huang, J. Magn. Magn. Mater. **51**, 1 (1985).
[16] S. Chikazumi, *Physics of Ferromagnetism*, 2nd ed. (Clarendon Press, Oxford, 1997).
[17] G. Scheunert, W. R. Hendren, A. A. Lapicki, P. Jesudoss, R. Hardeman, M. Gubbins, and R. M. Bowman, J. Phys. D **46**, 152001 (2013).
[18] J. Sláma, M. Šoka, A. Grusková, A. Gonzalez, and V. Jančárik, J. Electr. Eng. **62**, 239 (2011).
[19] K. Binder and A. P. Young, Rev. Mod. Phys. **58**, 801976 (1986).
[20] R. D. Noce, O. D. M. Gomes, S. D. de Magalhãs, W. Wolf, R. B. Guimarães, A. C. de Castro, M. J. M. Pires, W. A. A. Macedo, D. Givord, and V. M. T. S. Barthem, J. Appl. Phys. **106**, 093907 (2009).
[21] F. Yang, T. He, J. B. Chen, and F. Pan, J. Appl. Phys. **91**, 3114 (2002).
[22] R. Morales, M. Vélez, O. Petracic, I. V. Roshchin, Z-P. Li, X. Batlle, J. M. Alameda, and Ivan K. Schuller, Appl. Phys. Lett. **95**, 092503 (2009).
[23] A. Paul, C. Schmidt, N. Paul, A. Ehresmann, S. Mattauch, and P. Böni, Phys. Rev. B **86**, 094420 (2012).
[24] W. D. Corner, H. Bareham, R. L. Smith, F. M. Saad, B. K. Tanner, S. Farrant, D. W. Jones, B. J. Beaudry, and K. A. Gschneidner, Jr., J. Magn. Magn. Mater. **15**, 1488 (1980).
[25] B. P. Toperverg, in *Polarized Neutron Scattering*, Matter and Materials, Vol. 12 (Forschungszentrum Jülich, Germany, 2002), p. 247.
[26] V. R. Shah, C. Schanzer, P. Böni, and H. B. Braun, Phys. Met. Metallogr. **101**, S73 (2006); H. Xi and R. M. White, Phys. Rev. B **61**, 80 (2000).
[27] Ch. Kittel, Einführung in die Festkörperphysik, R. Oldenbourg Verlag, München, Wien, 12 (1999).

[28] N. I. N. Hosoito and H. Hashizume, J Phys. Condens. Matter. **14**, 5289 (2002); H. Hoffmann and R. Scherschlicht, in *Festkörperprobleme*, edited by R. Helbig (Vieweg, Braunschweig/Wiesbaden, 1998), p. 275.

[29] B. Spunzar and B. Kozarzewski, Phys. Status Solidi B **82**, 205 (1977).

[30] M. S. S. Brooks, O. Eriksson, and B. Johansson, J. Phys.: Condens. Matter **1**, 5861 (1989).

[31] J. F. Bobo, L. Gabillet, and M. Bibes, J. Phys. Condens. Matter **16**, S471 (2004).

[32] J. Ye, W. He, Q. Wu, H.-L. Liu, X.-Q. Zhang, Z.-Y. Chen, and Z.-H. Cheng, Sci. Rep. **3**, 2148 (2013).

[33] S. Sakshath, S. V. Bhat, P. S. Anil Kumar, D. Sander, and J. Kirschner, J. Appl. Phys. **109**, 07C114 (2011).

[34] C. Schubert, B. Hebler, H. Schletter, A. Liebig, M. Daniel, R. Abrudan, F. Radu, and M. Albrecht, Phys. Rev. B **87**, 054415 (2013).